bioRxiv preprint doi: https://doi.org/10.1101/2021.05.19.444883; this version posted May 28, 2021. The copyright holder for this preprint (which was not certified by peer review) is the author/funder, who has granted bioRxiv a license to display the preprint in perpetuity. It is made available under aCC-BY-NC-ND 4.0 International license.

Title:

Near-infrared imaging in fission yeast by genetically encoded biosynthesis of phycocyanobilin

Running Title:

iRFP imaging in fission yeast

Authors:

Keiichiro Sakai,[1,2,3] Yohei Kondo,[1,2,3] Hiroyoshi Fujioka,[4] Mako Kamiya,[5] Kazuhiro Aoki,[1,2,3,*] , and Yuhei Goto,[1,2,3,6*]

Affiliations:

[1]Quantitative Biology Research Group, Exploratory Research Center on Life and Living Systems (ExCELLS), National Institutes of Natural Sciences, 5-1 Higashiyama, Myodaiji-cho, Okazaki, Aichi 444-8787, Japan.

[2]Division of Quantitative Biology, National Institute for Basic Biology, National Institutes of Natural Sciences, 5-1 Higashiyama, Myodaiji-cho, Okazaki, Aichi 444-8787, Japan.

[3]Department of Basic Biology, School of Life Science, SOKENDAI (The Graduate University for Advanced Studies), 5-1 Higashiyama, Myodaiji-cho, Okazaki, Aichi 444-8787, Japan.

[4]Graduate School of Pharmaceutical Sciences, The University of Tokyo, 7-3-1 Hongo, Bunkyo-ku, Tokyo 113-0033, Japan.

[5]Graduate School of Medicine, The University of Tokyo, 7-3-1 Hongo, Bunkyo-ku, Tokyo 113-0033, Japan

[6]Lead contact

*Corresponding authors

*Correspondence: k-aoki@nibb.ac.jp and y-goto@nibb.ac.jp

KEYWORDS:

fission yeast, iRFP, biliverdin, phycocyanobilin, imaging

bioRxiv preprint doi: https://doi.org/10.1101/2021.05.19.444883; this version posted May 28, 2021. The copyright holder for this preprint (which was not certified by peer review) is the author/funder, who has granted bioRxiv a license to display the preprint in perpetuity. It is made available under aCC-BY-NC-ND 4.0 International license.

ABSTRACT

Near-infrared fluorescent protein (iRFP) is a bright and stable fluorescent protein with excitation and emission maxima at 690 nm and 713 nm, respectively. Unlike the other conventional fluorescent proteins such as GFP, iRFP requires biliverdin (BV) as a chromophore because iRFP originates from phytochrome. Here, we report that phycocyanobilin (PCB) functions as a brighter chromophore for iRFP than BV, and biosynthesis of PCB allows live-cell imaging with iRFP in the fission yeast *Schizosaccharomyces pombe*. We initially found that fission yeast cells did not produce BV, and therefore did not show any iRFP fluorescence. The brightness of iRFP attached to PCB was higher than that of iRFP attached to BV *in vitro* and in fission yeast. We introduced SynPCB, a previously reported PCB biosynthesis system, into fission yeast, resulting in the brightest iRFP fluorescence. To make iRFP readily available in fission yeast, we developed an endogenous gene tagging system with iRFP and all-in-one integration plasmids, which contain genes required for the SynPCB system and the iRFP-fused marker proteins. These tools not only enable the easy use of iRFP in fission yeast and the multiplexed live-cell imaging in fission yeast with a broader color palette, but also open the door to new opportunities for near-infrared fluorescence imaging in a wider range of living organisms.

bioRxiv preprint doi: https://doi.org/10.1101/2021.05.19.444883; this version posted May 28, 2021. The copyright holder for this preprint (which was not certified by peer review) is the author/funder, who has granted bioRxiv a license to display the preprint in perpetuity. It is made available under aCC-BY-NC-ND 4.0 International license.

INTRODUCTION

Fluorescent proteins (FPs) have become indispensable to visualize the biological processes in living cells and tissues (Lambert, 2019). Green fluorescent protein (GFP), the most widely used FP, has been intensively modified to improve the brightness and the photo-, thermo-, and pH-stabilities, and to change the excitation and emission spectrum. Use of a variety of fluorescent proteins with different excitation and emission spectra enables multiplexed fluorescence imaging to monitor multiple biological events simultaneously at high spatial and temporal resolution.

Near-infrared fluorescent proteins have been developed through the engineering of phytochromes, which are photosensory proteins of plants, bacteria, and fungi (Chernov et al., 2017). RpBphP2 from photosynthetic bacteria was engineered as an iRFP (later renamed iRFP713) by truncation and the saturation mutagenesis (Filonov et al., 2011). Since the initial report of iRFP, tremendous efforts have been devoted to developing near-infrared FPs with higher brightness, monomer formation, and longer wavelength (Filonov et al., 2011; Fushimi et al., 2019; Kamper et al., 2018; Matlashov et al., 2020; Oliinyk et al., 2019; Rodriguez et al., 2016; Rogers et al., 2019; Shcherbakova and Verkhusha, 2013; Shcherbakova et al., 2016; Shcherbakova et al., 2018; Stepanenko et al., 2016; Yu et al., 2014; Yu et al., 2015). Unlike the canonical fluorescent proteins derived from jellyfish or coral, phytochromes require a linear tetrapyrrole as a chromophore such as biliverdin IXα (BV), phycocyanobilin (PCB), or phytochromobilin (PΦB); the phytochromes autocatalytically form a covalent bond with the chromophore (Fushimi and Narikawa, 2021). These linear tetrapyrroles are produced from heme. Heme-oxygenase (HO) catalyzes oxidative cleavage of heme to generate BV with the help of ferredoxin (Fd), an electron donor, and ferredoxin-NADP+ reductase (Fnr). In cyanobacteria, PCB is produced from BV through PcyA, Fd, and Fnr, while in higher plants PΦB is synthesized from BV using HY2, Fd, and Fnr. To exploit phytochromes that are required for PCB or PΦB in other organisms, our group and others have demonstrated reconstitution of BV, PCB, and PΦB synthesis in bacteria, mammalian cells, frog eggs, the budding yeast, *Pichia*, and fission yeast (Gambetta and Lagarias, 2001; Hochrein et al., 2017; Kyriakakis et al., 2018; Landgraf et al., 2001; Mukougawa et al., 2006; Müller et al., 2013; Shin et al., 2014; Tooley et al., 2001; Uda et al., 2017).

As the fluorescence of iRFP depends on the chromophore formation, the BV concentration is of critical importance for imaging iRFP (Fig. 1A). Indeed, it has been reported that the addition of purified BV increases the fluorescence of iRFPs (Piatkevich et al., 2017; Shemetov et al., 2017). Alternatively, genetic modifications such as the overexpression of heme oxygenase-1 (HO1), which

bioRxiv preprint doi: https://doi.org/10.1101/2021.05.19.444883; this version posted May 28, 2021. The copyright holder for this preprint (which was not certified by peer review) is the author/funder, who has granted bioRxiv a license to display the preprint in perpetuity. It is made available under aCC-BY-NC-ND 4.0 International license.

catalyzes heme to generate BV, and the knock out of biliverdin reductase A (BVRA), which degrades BV to generate bilirubin, improve the brightness of iRFP through the additional accumulation of BV (Kobachi et al., 2020; Shemetov et al., 2017). On the other hand, because *Caenorhabditis elegans* produces little or no BV (Ding et al., 2017), it is not possible to image biological processes in this nematode simply by introducing the iRFP gene. In the case of multicellular organisms that cannot produce BV including *C.elegans*, the introduction of genes required for BV production is more effective than the external addition of BV, because of the low tissue penetration property. However, at present, only the introduction of the HO1 gene has been reported as a genetically encoded method for inducing the iRFP chromophore, and it has not been improved or optimized yet.

Here, we report that PCB acts as a better chromophore for iRFP than BV, and genetically encoded PCB synthesis outperforms HO1-mediated BV production in terms of iRFP brightness in fission yeast. We accidentally found that iRFP did not fluoresce in fission yeast because of the lack of the HO1 gene, and therefore the lack of BV. Both the external BV addition and heterologous HO1 expression rendered iRFP fluorescent in fission yeast. To our surprise, PCB biosynthesis with a SynPCB system, which we have previously reported (Uda et al., 2017; Uda et al., 2020), and treatment of the purified PCB yielded brighter iRFP fluorescence than that by either BV biosynthesis or BV treatment. We confirmed that PCB-bound iRFP showed higher fluorescence quantum yield than BV-bound iRFP. To facilitate the simple use of iRFP in fission yeast, we developed a plasmid for iRFP tagging of endogenous proteins at the C-terminus, novel genome integration vectors, and all-in-one plasmids carrying genes required for both the SynPCB system and iRFP-fused marker proteins.

bioRxiv preprint doi: https://doi.org/10.1101/2021.05.19.444883; this version posted May 28, 2021. The copyright holder for this preprint (which was not certified by peer review) is the author/funder, who has granted bioRxiv a license to display the preprint in perpetuity. It is made available under aCC-BY-NC-ND 4.0 International license.

RESULTS

iRFP does not fluoresce in fission yeast *Schizosaccharomyces pombe*

During the process of experiments, we accidentally found that iRFP did not fluoresce at all in fission yeast. We first tested whether iRFP was applicable to near-infrared imaging in fission yeast. We established a cell strain stably expressing nuclear localization signal (NLS)-iRFP-NLS under the constitutive promoter *Padh1*. No iRFP fluorescence was observed at an excitation wavelength of 640 nm (Fig. 1B). Because the iRFP requires BV as a chromophore for emitting fluorescence (Fig. 1A), we hypothesized that fission yeast could not metabolize BV intracellularly. Upon the addition of external BV, the nuclear iRFP fluorescence signal was recovered (Fig. 1B). The titration of BV concentration yielded a dose-dependent increase in iRFP fluorescence up to 125 μM (Fig. 1C). We next examined the kinetics of BV incorporation into fission yeast cells. Treatment with a high dose of BV (500 μM) gradually increased iRFP fluorescence with a plateau in fluorescence at 60-120 min after the treatment (Fig. 1D). Since BV is produced from heme through HO, we searched for *HO* in the genomes of fission yeast and representative fungal species. As expected, we could not find any *HO* or *HO*-like gene in fission yeast (Fig. S1). Interestingly, *HO* and/or *HO*-like genes, which have been found from bacteria to higher eukaryotes, are frequently and sporadically lost in the representative fungal species (Fig. S1). Indeed, while iRFP has been widely used in the budding yeast, *Saccharomyces cerevisiae*, which retains an *HO* gene (Geller et al., 2019; Li et al., 2017; Tojima et al., 2019; Wosika et al., 2016), there have been no studies using iRFP in the fission yeast, *S.pombe*. Taken together, these facts led us to conclude that iRFP does not fluoresce in fission yeast due to the lack of BV and *HO*.

bioRxiv preprint doi: https://doi.org/10.1101/2021.05.19.444883; this version posted May 28, 2021. The copyright holder for this preprint (which was not certified by peer review) is the author/funder, who has granted bioRxiv a license to display the preprint in perpetuity. It is made available under aCC-BY-NC-ND 4.0 International license.

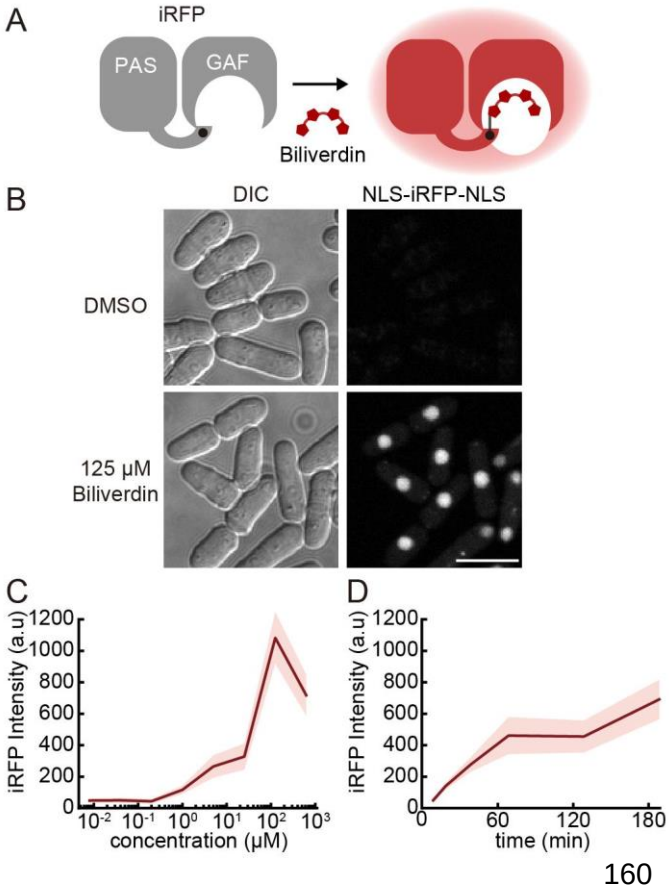

Fig 1. iRFP does not fluoresce in fission yeast. (A) Schematic illustration of chromophore formation of iRFP with biliverdin (BV). BV covalently attaches to iRFP as a chromophore. The PAS domain in iRFP contains a conserved cysteine residue at the N-terminus that covalently attaches to the BV, while the BV itself fits into the cleft in the GAF domain. (B) Representative images of fission yeast expressing NLS-iRFP-NLS with or without external BV treatment. Scale bar, 10 μm. (C) Dose-response curve of iRFP fluorescence as a function of levels of BV incorporation in fission yeast cells. Fission yeast cells were cultured in liquid YEA and incubated at room temperature for 3 h with the indicated concentration of BV (8 nM, 40 nM, 200 nM, 1 μM, 5 μM, 25 μM, 125 μM, and 625 μM). The red line and shaded area indicate the averaged intensity and S.D., respectively (n = 50 cells). (D) Time-course of BV incorporation into fission yeast cells. Fission yeast cells were cultured in liquid YEA and treated with 500 μM BV at the time zero. The red line and shaded area indicate the averaged intensity and S.D., respectively (n = 50 cells).

Development of novel stable knock-in plasmids: pSKI

The above results showed that the external supply of BV required high dose and long-term incubation (60–120 min) to realize iRFP fluorescence in fission yeast, which prompted us to seek an alternative route to iRFP fluorescence by introducing genes for the biosynthesis of BV. Before starting to develop the reconstitution system, we developed novel stable integration vectors that met our specific requirements—stable one copy integration into the genome, no effect on the auxotrophy of integrated cells, and distant integration loci for crossing strains—rather than using one of the previously developed integration systems (Fennessy et al., 2014; Kakui et al., 2015; Keeney and Boeke, 1994; Matsuyama et al., 2004; Maundrell, 1993; Siam et al., 2004; Vještica et al., 2020). At first, we chose three gene-free loci on each chromosome at chromosome I positions 1,508,522 to 1,508,641 (near *mug165*, 1L), chromosome II positions 447,732 to 447,827 (near *pho4*, 2L), and chromosome III positions 1,822,244 to 1,822,343 (near *nup60*, 3R) (Fig. S2A). Next, we designed and developed plasmids that contain genes required for replication and amplification in *E. coli* (*Amp*, ori), the constitutive promoter *Padh1* or inducible promoter *Pnmt1*, a multiple cloning site (MCS), an *adh1*

bioRxiv preprint doi: https://doi.org/10.1101/2021.05.19.444883; this version posted May 28, 2021. The copyright holder for this preprint (which was not certified by peer review) is the author/funder, who has granted bioRxiv a license to display the preprint in perpetuity. It is made available under aCC-BY-NC-ND 4.0 International license.

terminator, a selection marker cassette encoding an antibiotic-resistance gene for fission yeast, and homology arms connected with the one-cut restriction enzyme recognition site for plasmid linearization (Fig. S2B). Expected genomic integration with these vectors was confirmed by genomic PCR using primers designed to span the integration boundary (Fig. S2C). None of these integrations affected the bulk growth of fission yeast (Fig. S2D), and the protein expression levels from these three loci were comparable or moderately higher than that from the Z-locus (Fig. S2E). We named this series of plasmids using the prefix pSKI (plasmid for Stable Knock-In, also see Table S1) and used them for the following experiments.

PCB brightens iRFP more efficiently than BV in fission yeast

HO is the crucial enzyme in the BV biosynthesis pathway, catalyzing the linearization of tetrapyrrole (Fig. 2A). Therefore, we established fission yeast cells stably expressing HO1 and NLS-iRFP-NLS with pSKI, and quantified the resulting iRFP fluorescence. As expected, the expression of HO1 derived from *Thermosynechococcus elongatus* BP-1 in mitochondria, where heme is abundant, demonstrated iRFP fluorescence, and the iRFP fluorescence was brighter than that achieved by the external addition of BV (Fig. 2B, second and third columns). Because HO1 is known to catalyze heme in the presence of reduced Fd (Rhie and Beale, 1992), we next examined whether co-expression of HO1 and tFnr-Fd, a chimeric protein of truncated Fnr and Fd (Uda et al., 2020), would improve HO1-mediated iRFP fluorescence. However, the co-expression of HO1 and tFnr-Fd in mitochondria did not further enhance iRFP fluorescence as compared to the expression of only HO1 (Fig. 2B, sixth column), suggesting that authentic ferredoxin in fission yeast sufficiently supports the catalytic reaction through HO1.

Unexpectedly, in a series of experiments, we found a further increment in iRFP fluorescence by PCB (Fig. 2B, ninth column). When PcyA, the enzyme responsible for the production of PCB from BV, was co-expressed with HO1 and tFnr-Fd, the level of iRFP fluorescence was higher than other conditions (Fig. 2B, ninth column). To validate these results, we treated the cells expressing NLS-iRFP-NLS with purified PCB instead of BV. The addition of external PCB substantially outperformed the addition of BV with respect to iRFP fluorescence intensity (Fig. 2C and 2D). While the fluorescence intensities were quite different between PCB-bound iRFP (iRFP-PCB) and BV-bound iRFP (iRFP-BV), the effective concentration of the dose-response curve (Fig. 1C and 2C) and the kinetics of chromophore incorporation (Fig. 1D and 2D) were comparable between them.

bioRxiv preprint doi: https://doi.org/10.1101/2021.05.19.444883; this version posted May 28, 2021. The copyright holder for this preprint (which was not certified by peer review) is the author/funder, who has granted bioRxiv a license to display the preprint in perpetuity. It is made available under aCC-BY-NC-ND 4.0 International license.

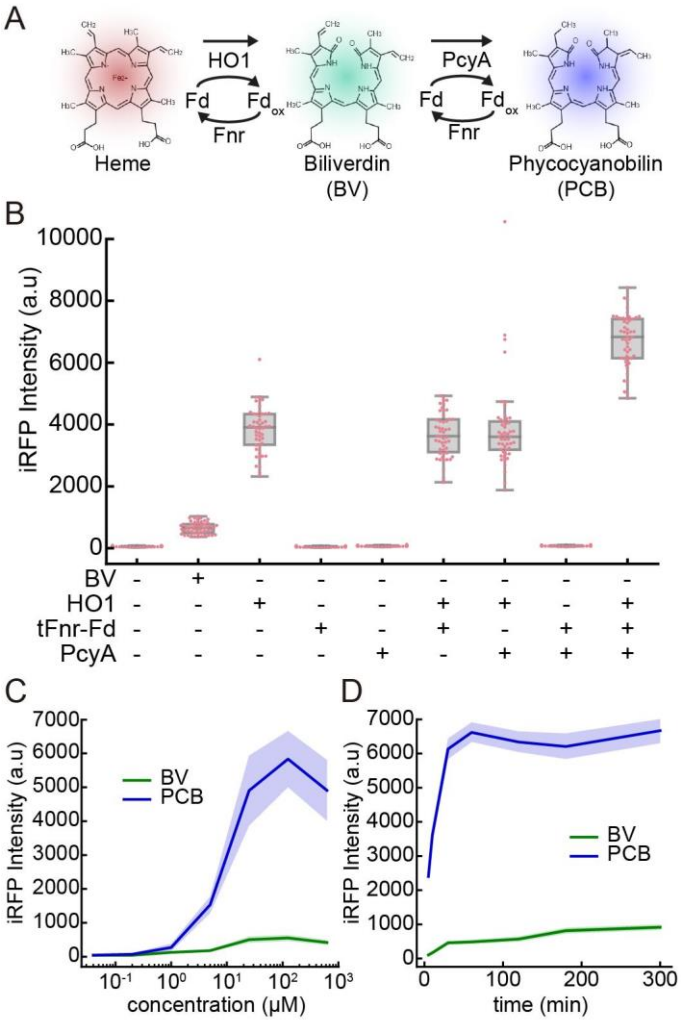

Fig 2. PCB brightens iRFP more efficiently than BV in fission yeast.
(A) Schematic illustration of the PCB biosynthesis pathway. (B) Quantification of iRFP fluorescence in fission yeast cells expressing HO1, tFnr-Fd, and PcyA. Under the BV condition, cells were treated with 125 μM BV for 1 h at room temperature. Each dot represents iRFP fluorescence from a single cell with a boxplot, in which the box shows the quartiles of data with the whiskers denoting the minimum and maximum except for the outliers detected by 1.5 times the interquartile range (n = 50 cells). (C) Dose-response curve of iRFP fluorescence as a function of the levels of BV or PCB incorporation in fission yeast cells. Fission yeast cells were cultured in liquid YEA and incubated at room temperature for 3 h with the indicated concentration of BV or PCB (8 nM, 40 nM, 200 nM, 1 μM, 5 μM, 25 μM, 125 μM, and 625 μM). The lines and shaded areas indicate the averaged intensities and S.D., respectively (n = 50 cells). (D) Time-course of iRFP fluorescence in response to BV or PCB treatment. Fission yeast cells were cultured in liquid YEA and treated with 125 μM BV or PCB at time zero. The lines and shaded areas indicate the averaged intensities and S.D., respectively (n = 50 cells).

PCB yields brighter fluorescence as an iRFP chromophore than BV

The above data indicated the possibility that PCB might be a more suitable chromophore for iRFP than BV. To prove this hypothesis, we first examined whether the efficiency of holo-iRFP formation accounted for the difference in iRFP fluorescence between BV- and PCB-treated cells. PCB was added to the cells with HO1 expression, which exhibited constant intracellular production of BV. Therefore, iRFP has already formed a holo-complex with BV before attaching to PCB (Fig. 3A). Given that iRFP-PCB is brighter than iRFP-BV, we reasoned that HO1 expression attenuated the increase in iRFP fluorescence when the cells were further treated with purified PCB due to the competition between the PCB and already existing BV for binding to iRFP. As we expected, the addition of purified PCB hardly increased iRFP fluorescence in cells that had been expressing HO1, in spite of the dose-dependent

bioRxiv preprint doi: https://doi.org/10.1101/2021.05.19.444883; this version posted May 28, 2021. The copyright holder for this preprint (which was not certified by peer review) is the author/funder, who has granted bioRxiv a license to display the preprint in perpetuity. It is made available under aCC-BY-NC-ND 4.0 International license.

increase in iRFP fluorescence by PCB treatment in cells not expressing HO1 (Fig. 3B and 3C). These observations reveal that almost all iRFP forms a holo-complex with BV when HO1 is expressed.

To understand why iRFP-PCB was brighter than iRFP-BV, we prepared recombinant iRFP expressed in *E. coli* and purified apo-iRFP (Filonov et al., 2011) (Fig. S3A). Apo-iRFP was mixed with PCB and BV to form holo-iRFP, *i.e.*, iRFP-PCB and iRFP-BV, respectively (Fig. S3B). Binding of PCB to iRFP resulted in a change in the absorption spectrum from the free PCB (Fig. 3D). The absorbance maximum of iRFP-PCB was 10 nm blue-shifted from that of iRFP-BV (Fig. 3E). Fluorescence excitation and emission spectra were also 10 nm blue-shifted in iRFP-PCB compared to iRFP-BV (Fig. S3C and S3D). Notably, the fluorescence quantum yield of iRFP-PCB was nearly twice as high as that of iRFP-BV (0.094 vs. 0.054), while their molecular extinction coefficient values were comparable (Fig. 3F). Based on these results, we concluded that iRFP forms a complex with PCB as a holo-form and that iRFP-PCB is brighter than iRFP-BV at the molecular level.

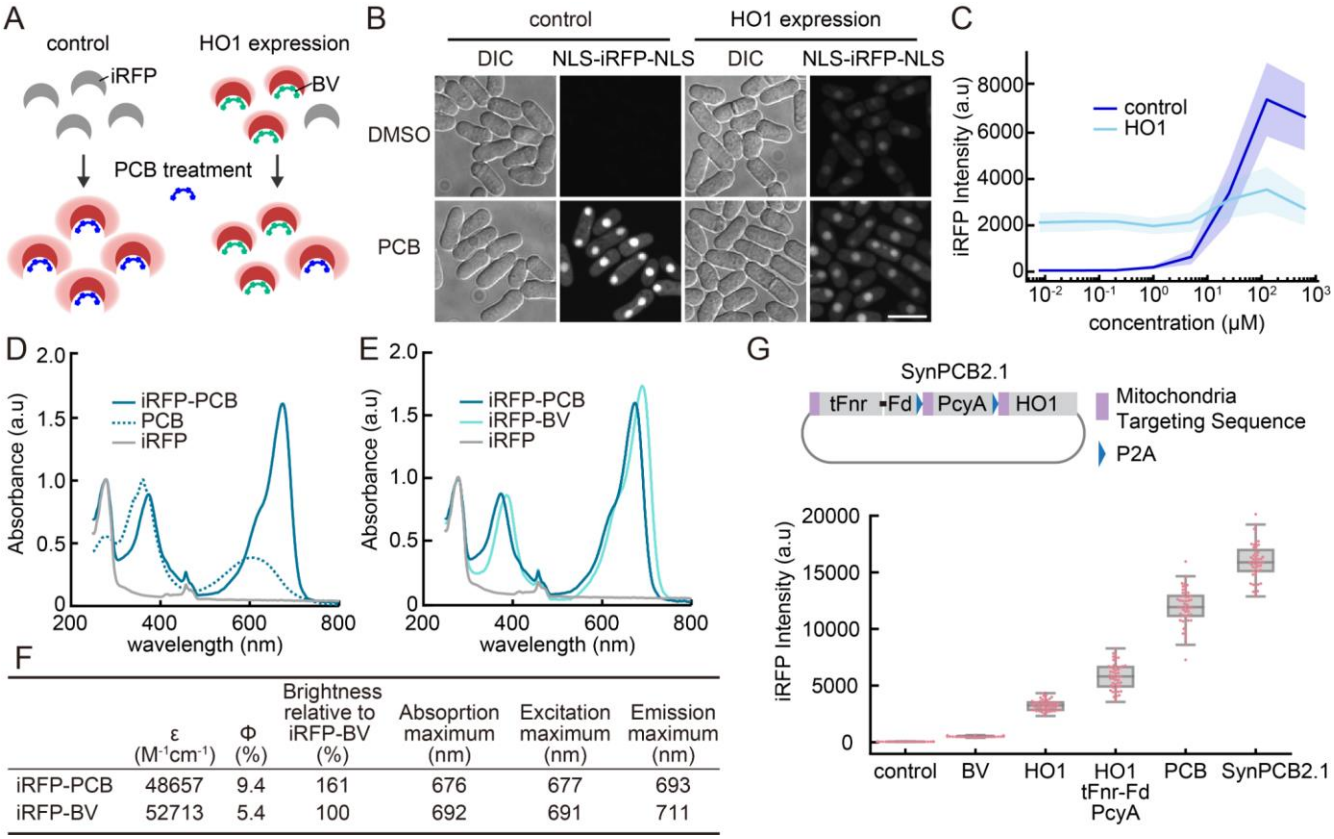

F

	ε ($M^{-1}cm^{-1}$)	Φ (%)	Brightness relative to iRFP-BV (%)	Absoprtion maximum (nm)	Excitation maximum (nm)	Emission maximum (nm)
iRFP-PCB	48657	9.4	161	676	677	693
iRFP-BV	52713	5.4	100	692	691	711

Fig 3. PCB yields brighter fluorescence as an iRFP chromophore than BV

(A) Schematic illustration of the experimental procedure. In control fission yeast cells, iRFP shows fluorescence upon the addition of PCB. In HO1 expressing cells, BV binds to iRFP as a chromophore before the addition of PCB. Therefore, BV competes with PCB for binding to iRFP. (B) Representative images of fission yeast expressing NLS-iRFP-NLS with or without external PCB (125 μM) treatment. Scale bar, 10 μm. (C) Dose-response curve of iRFP fluorescence as a function of the PCB

bioRxiv preprint doi: https://doi.org/10.1101/2021.05.19.444883; this version posted May 28, 2021. The copyright holder for this preprint (which was not certified by peer review) is the author/funder, who has granted bioRxiv a license to display the preprint in perpetuity. It is made available under aCC-BY-NC-ND 4.0 International license.

concentration in a culture of fission yeast cells.. Fission yeast cells were cultured in liquid YEA and incubated at room temperature for 1 h with the indicated concentration of PCB (8 nM, 40 nM, 200 nM, 1 μM, 5 μM, 25 μM, 125 μM, and 625 μM). The lines and shaded areas indicate the averaged intensities and S.D., respectively (n = 50 cells). (D) Normalized absorption spectra of PCB-bound iRFP (iRFP-PCB), free PCB, or iRFP. First, the spectra of iRFP-PCB and iRFP were normalized based on the absorbance at 280 nm (absorbance of protein), followed by normalization of the PCB spectrum by the absorbance at 375 nm. (E) Normalized absorption spectra of iRFP-PCB, BV-bound iRFP (iRFP-BV), and iRFP. The absorption spectra were normalized by the absorbance at 280 nm of each spectrum. (F) Summary of the fluorescence properties of iRFP-PCB and iRFP-BV *in vitro*. Φ and ε represent the fluorescence quantum yield and molar extinction coefficient, respectively. (G) (upper) Structure of the SynPCB2.1 plasmid expressing tFnr-Fd, PcyA, and HO1. These proteins are tagged with the mitochondria targeting sequence (MTS) at their N-termini and flanked by P2A, a self-cleaving peptide. (lower) Quantification of iRFP fluorescence under the indicated conditions. Cells were treated with 125 μM BV or PCB for 1 h at room temperature (second and fifth columns). Each dot represents iRFP fluorescence of a single-cell with a boxplot, in which the box shows the quartiles of data with the whiskers denoting the minimum and maximum except for the outliers detected by 1.5 times the interquartile range (n = 50 cells).

SynPCB2.1 is ideal for iRFP imaging in fission yeast

For easy iRFP imaging using PCB as a chromophore, we introduced a system for efficient PCB biosynthesis, SynPCB2.1, in which the *tFnr-Fd*, *PcyA*, and *HO1* genes are tandemly fused with the cDNAs of the mitochondrial targeting sequences (MTS) at their N-termini, and flanked by self-cleaving P2A peptide cDNAs for multicistronic gene expression (Uda et al., 2020) (Fig. 3H). The single-cassette of SynPCB2.1 genes was knocked-in into cells expressing NLS-iRFP-NLS with a pSKI vector system, and expressed under the *adh1* promoter. The cells expressing SynPCB2.1 showed higher iRFP fluorescence than either cells treated with PCB or cells expressing the three genes individually (Fig. 3H). To determine whether and to what extent iRFP formed a complex with PCB or BV in the cells, we measured the emission spectrum of iRFP in a living cell. As for the emission spectrum *in vitro*, the cells showed a distinct emission spectrum between iRFP-PCB and iRFP-BV, namely, a blue-shifted emission spectrum of iRFP-PCB (Fig. S4A). A similar shift was observed when the emission spectrum of cells expressing SynPCB2.1 was compared to that of cells expressing HO1 (Fig. S4B and summarized in Fig. S4E). Importantly, cells separately expressing HO1, tFnr-Fd, and PcyA exhibited an intermediate emission spectrum, suggesting a mixture of iRFP-BV and iRFP-PCB in this cell line. The presence of iRFP-BV would explain why iRFP fluorescence by SynPCB2.1 was brighter than that generated by separate expression of the three enzymes in fission yeast (Fig. 3G). Moreover, the emission spectra obtained from living fission yeast cells demonstrated that iRFP-PCB was much brighter than iRFP-BV (Fig. S4C and S4D). From these data, we concluded that PCB biosynthesis by SynPCB2.1 is ideal for iRFP imaging in fission yeast.

bioRxiv preprint doi: https://doi.org/10.1101/2021.05.19.444883; this version posted May 28, 2021. The copyright holder for this preprint (which was not certified by peer review) is the author/funder, who has granted bioRxiv a license to display the preprint in perpetuity. It is made available under aCC-BY-NC-ND 4.0 International license.

During iRFP imaging experiments, we found that PCB synthesized in fission yeast cells expressing SynPCB2.1 is leaked out of the cells and incorporated into the surrounding cells. To clearly show the PCB leakage, we co-cultured cells expressing only SynPCB2.1 and cells expressing only NLS-iRFP-NLS. While neither strains exhibited any fluorescence when cultured singly, NLS-iRFP-NLS emanated fluorescence when cells were co-cultured with the cells expressing SynPCB2.1 (Fig. S5B and S5C). The data indicate that in fission yeast PCB is leaked into the extracellular space.

iRFP imaging in fission yeast: Development of endogenous tagging and all-in-one integration systems.

To further exploit the advantages of iRFP imaging in fission yeast, we first established C-terminal tagging plasmids based on a commonly used PCR-based tagging system (Longtine et al., 1998). The plasmids included an *iRFP* cassette followed by one of four different selection markers (Fig. 4A). By using these plasmids, we verified endogenous *iRFP* tagging to several genes including *cdc2* (CDK, nucleus), *rpb9* (PolII, chromatin), *rpa49* (PolI, nucleolus), *swi6* (heterochromatin), *pds5* (cohesin), *cut11* (nuclear envelope), *mal3* (microtubule plus-end), *sfi1* (spindle pole body, SPB), *cox4* (mitochondria), and *cnx1* (endoplasmic reticulum, ER) with the expression of SynPCB2.1. All tested proteins showed the expected subcellular localization in fission yeast (Fig. 4B), although the signal-to-noise ratios were dependent on the expression level of the endogenous tagged proteins.

bioRxiv preprint doi: https://doi.org/10.1101/2021.05.19.444883; this version posted May 28, 2021. The copyright holder for this preprint (which was not certified by peer review) is the author/funder, who has granted bioRxiv a license to display the preprint in perpetuity. It is made available under aCC-BY-NC-ND 4.0 International license.

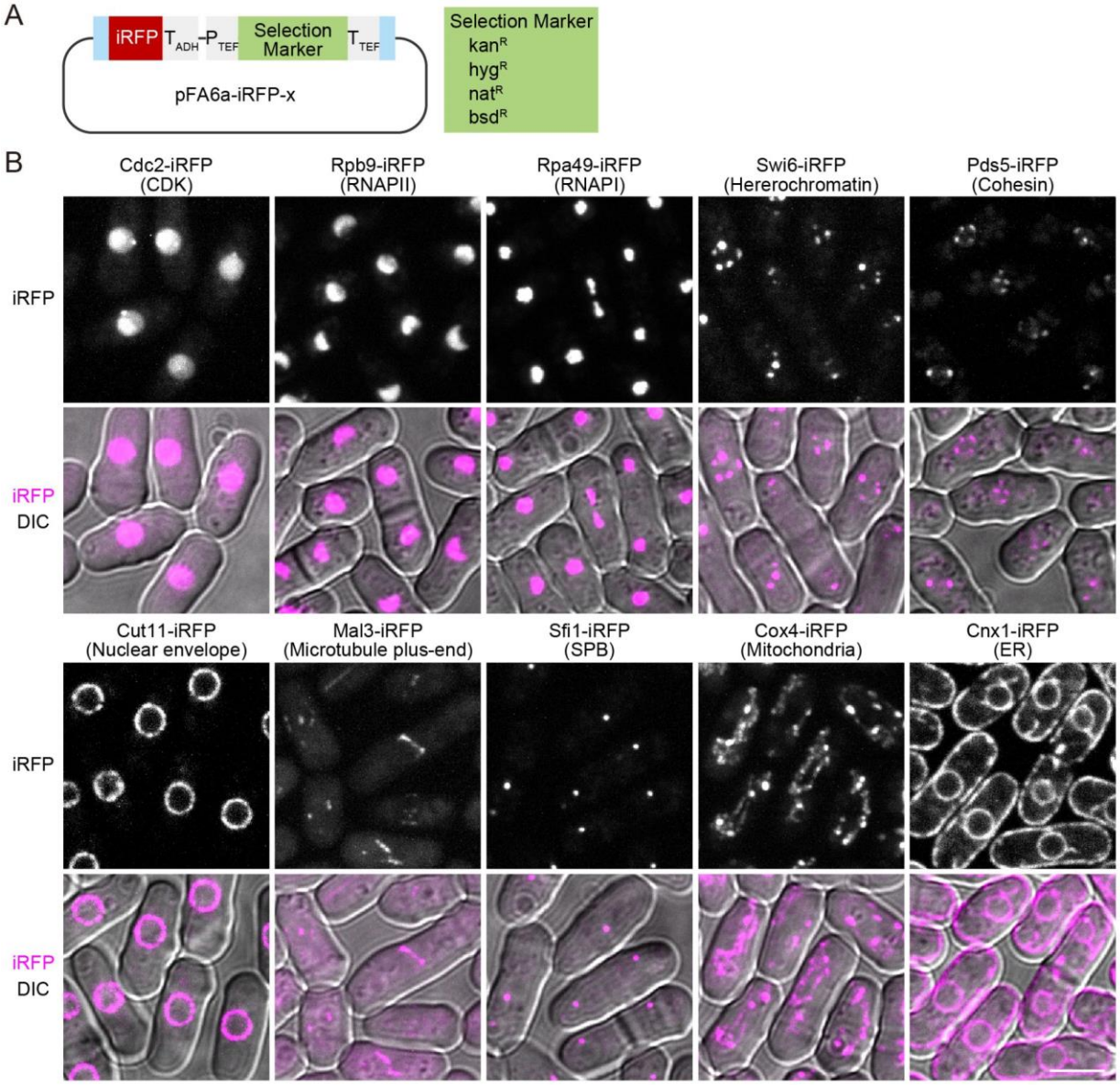

Fig 4. Visualization of endogenous proteins by iRFP in fission yeast
(A) Schematic illustration of the plasmid for iRFP tagging of endogenous proteins at the C-terminus. Cyan boxes indicate the common overlapping sequences (Longtine et al., 1998). The plasmid list is shown in Table S1. (B) The subcellular localization of endogenous proteins tagged with iRFP using pFa6a-iRFP. iRFP signals are shown in grayscale in the upper panels, and DIC images are merged with magenta iRFP signals and shown in the lower panels. Maximal projection images for iRFP are shown except for Cut11-iRFP and Cnx1-iRFP. Scale bar, 5 μm.

Second, we developed all-in-one plasmids carrying SynPCB2.1 and iRFP fusion protein genes to avoid a situation in which these two genes occupy two of the limited selection markers and integration loci. As a proof-of-concept, we introduced cDNA of Lifeact-iRFP (F-actin marker) or NLS-iRFP-NLS (nucleus marker) into the pSKI plasmid with the SynPCB2.1 gene cassette (Fig. 5A and

bioRxiv preprint doi: https://doi.org/10.1101/2021.05.19.444883; this version posted May 28, 2021. The copyright holder for this preprint (which was not certified by peer review) is the author/funder, who has granted bioRxiv a license to display the preprint in perpetuity. It is made available under aCC-BY-NC-ND 4.0 International license.

5B). Fission yeast transformed with these plasmids displayed the bright F-actin pattern including actin patches, actin cables, and contractile ring (Fig. 5A) and nucleus (Fig. 5B). Taking full advantage of iRFP imaging with the SynPCB system in fission yeast, we established cells expressing four different proteins: The nucleus, plasma membrane, kinetochore, tubulin, and F-actin were labeled with NLS-mTagBFP2, Turquoise2-GL-ras1ΔN200, endogenous Mis12-mNeonGreen, mCherry-Atb2, and Lifeact-iRFP, respectively (Fig. 5C).

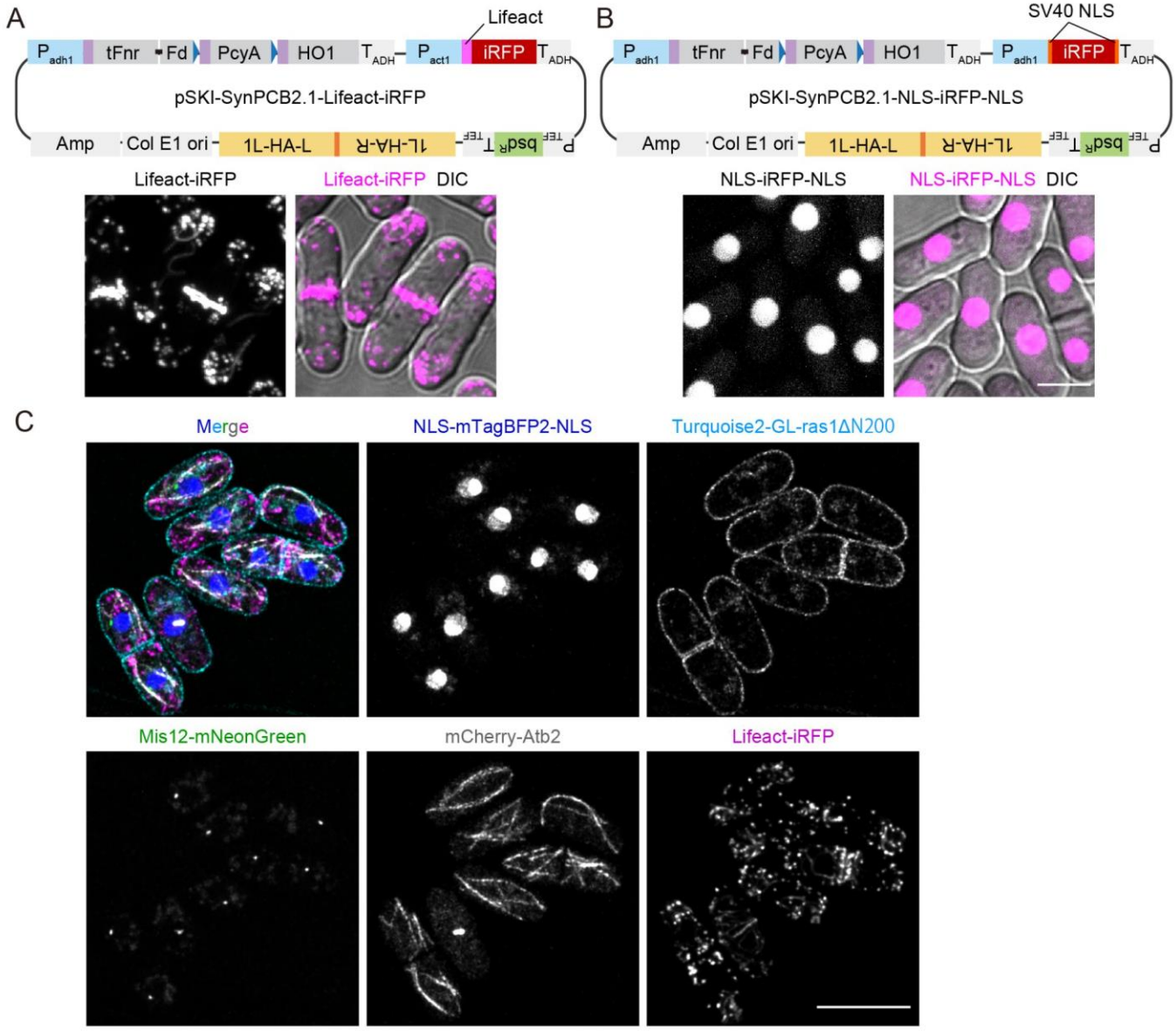

Fig 5. All-in-one plasmids for iRFP imaging

(A) (upper) Schematic illustration of 1L locus integration plasmids for the expression of SynPCB2.1 and Lifeact fused with iRFP (pSKI-SynPCB2.1-Lifeact-iRFP). (lower) Representative images of fission yeast expressing Lifact-iRFP are shown with the maximal intensity projection image and DIC-merged image. (B) (upper) Schematic illustration of 1L locus integration plasmids for the expression of SynPCB2.1 and NLS-iRFP-NLS (pSKI-SynPCB2.1-NLS-iRFP-NLS). (lower) Representative images

bioRxiv preprint doi: https://doi.org/10.1101/2021.05.19.444883; this version posted May 28, 2021. The copyright holder for this preprint (which was not certified by peer review) is the author/funder, who has granted bioRxiv a license to display the preprint in perpetuity. It is made available under aCC-BY-NC-ND 4.0 International license.

of fission yeast expressing NLS-iRFP-NLS are shown with the maximal intensity projection image and DIC-merged image. Scale bar, 5 μm. (C) Multiplexed imaging of fission yeast expressing NLS-mTagBFP2-NLS (nucleus), Turquoise2-GL-ras1ΔN200 (plasma membrane), Mis12-mNeonGreen (kinetochore), mCherry-Atb2 (tubulin), and Lifeact-iRFP (F-actin). Maximal intensity projection images (except for Turquoise2-GL-ras1ΔN200; single z-section) and a merged image are shown. Scale bar, 10 μm.

PCB can be used as a chromophore in mammalian cells

Finally, we tested whether PCB could be used as an iRFP chromophore in other organisms. HeLa cells expressing iRFP along with EGFP, an internal control for iRFP expression, were treated with external BV or PCB. PCB treatment increased the brightness of iRFP in HeLa cells to the same degree as BV treatment (Fig. S6A and S6B). BVRA KO HeLa cells displayed higher iRFP fluorescence than did parental HeLa cells, as reported previously (Kobachi et al., 2020), but did not show any change in iRFP fluorescence by BV or PCB treatment (Fig. S6B), probably because all iRFP molecules were occupied by BV. In contrast to fission yeast, the increment of iRFP fluorescence by PCB treatment was comparable to that by BV treatment in parental HeLa cells (Fig. S6B). Taken together, these results led us to conclude that PCB is applicable to iRFP imaging in mammalian cells, although it does not offer significant advantage over BV.

bioRxiv preprint doi: https://doi.org/10.1101/2021.05.19.444883; this version posted May 28, 2021. The copyright holder for this preprint (which was not certified by peer review) is the author/funder, who has granted bioRxiv a license to display the preprint in perpetuity. It is made available under aCC-BY-NC-ND 4.0 International license.

DISCUSSION

In this study, we demonstrated that iRFP does not fluoresce in fission yeast because of the lack of the BV-producing enzyme HO. Moreover, we found that PCB acts as a brighter chromophore for iRFP than BV both *in vitro* and in fission yeast expressing SynPCB2.1. Although PCB is not an authentic chromophore for iRFP nor the original RpBphP2, our data strongly suggested that PCB forms a fluorescent chromophore in iRFP. Finally, we developed endogenous iRFP tagging plasmids and all-in-one plasmids carrying SynPCB2.1 and iRFP marker proteins for the easy use of near-infrared imaging in fission yeast. As an alternative to external chromophore addition, the SynPCB2.1 system has potential advantages for iRFP imaging, including being fully genetically encoded and capable of providing even brighter iRFP fluorescence in fission yeast.

Our data indicate that PCB is more suitable as an iRFP chromophore than BV in fission yeast for several reasons. The first reason is that iRFP-PCB has 2-fold higher fluorescence quantum yield than iRFP-BV *in vitro*. The second reason is that the excitation and emission spectra of iRFP-PCB are blue-shifted in comparison to those of iRFP-BV. This result is consistent with previous works describing the blue-shifted spectra of PCB (Loughlin et al., 2016; Rumyantsev et al., 2015). The blue-shifted spectra of iRFP-PCB possess favorable properties for most conventional confocal microscopes, which are equipped with a 630–640 nm excitation laser for near-infrared fluorescence imaging. The third conceivable reason is the efficient chromophore formation. Indeed, RpBphP1-derived GAF-FP bound PCB 1.75-fold more efficiently than BV (Rumyantsev et al., 2015). In contrast to fission yeast, HeLa cells showed no difference in iRFP fluorescence between PCB and BV (Fig. S6). This could be partly due to the metabolism and culture conditions in mammalian cells, including synthesis of BV by endogenous HO1, degradation of BV and PCB by BVRA (Kobachi et al., 2020; Terry et al., 1993; Uda et al., 2017), and the presence of BV and bilirubin in the serum of the culture medium. Based on the results obtained by using fission yeast, we presume that the existence of BV within a HeLa cell and in the culture medium attenuates the increase in PCB-induced iRFP fluorescence. Moreover, other tetrapyrroles, such as primarily PPIX, could compete for iRFP with BV or PCB (Lehtivuori et al., 2013; Wagner et al., 2008).

The SynPCB system allows bright iRFP imaging without adding the external chromophores. This fact led us to consider that PCB might be applicable to other BV-based fluorescent proteins and optogenetic tools. Indeed, near-infrared fluorescent proteins that originate from cyanobacteriochrome, such as smURFP or iRFP670nano (Oliinyk et al., 2019; Rodriguez et al., 2016) exhibit high affinity to PCB because the original cyanobacteriochromes bind specifically to PCB. miRFPs including

bioRxiv preprint doi: https://doi.org/10.1101/2021.05.19.444883; this version posted May 28, 2021. The copyright holder for this preprint (which was not certified by peer review) is the author/funder, who has granted bioRxiv a license to display the preprint in perpetuity. It is made available under aCC-BY-NC-ND 4.0 International license.

miRFP670, miRFP703, and miRFP720 have also been developed from the bacterial phytochrome RpBphP1 (Shcherbakova et al., 2016; Shemetov et al., 2017), and therefore the SynPCB systems could be used for imaging with these miRFPs. Bacteriophytochrome-based optogenetic tools using BV (Kaberniuk et al., 2016; Monakhov et al., 2020; Qian et al., 2020; Redchuk et al., 2017) would be a potential target for the application of the SynPCB system. We should note that it is not clear whether PCB, instead of BV, increases the fluorescence brightness of these near-infrared fluorescent proteins and maintains the photoresponsive properties of these optogenetic tools. Fission yeast is an ideal model to assess phytochrome-based tools in a cell, such as the difference between BV and PCB as chromophores and the efficacy of genetically-encoded chromophore reconstruction, because there is neither a synthetic nor a degradation pathway of BV in fission yeast.

We found that the *HO* homologue is frequently lost in fungal species including the fission yeast during evolution (Fig. S1). In addition to fungi, *Caenorhabditis elegans*, one of the most popular model organisms, has shown very low, but not zero, BV-producing activity (Ding et al., 2017). Consistent with this fact, we could not find an *HO* homologue in the worm genome. The SynPCB system paves the way to utilizing iRFP for a broader range of organisms that lost an *HO* homologue during evolution. In addition, we recognized that PCB produced by SynPCB2.1 is leaked from the cells and taken up by surrounding cells, as evidenced by iRFP fluorescence (Fig. S5). It is possible that the same events take place under actual ecological conditions; some organisms may exploit tetrapyrroles produced by other organisms in order to render their own phytochromes functional. In fact, *Aspergillus nidulans* and *Neurospora crassa*, both of which lost an *HO* homologue in their genomes (Fig. S1), harbor phytochrome genes that are required for chromophores (Blumenstein et al., 2005; Froehlich et al., 2005). The exchanges of tetrapyrroles between living organisms might explain why the *HO* gene is sporadically lost in many organisms.

In this study, we have reported an iRFP imaging platform for fission yeast and a novel chromosome integration plasmid series, pSKI. The endogenous iRFP tagging system is based on a commonly used one, allowing anyone to introduce it quickly. The all-in-one plasmids carrying NLS-iRFP-NLS enable nuclear tracking without occupying green or red color fluorescence channels and automatic analysis of large-scale time-lapse images with nuclear translocation-type sensors (Regot et al., 2014). Further characterization and engineering will result in wide use of iRFP and phytochrome-based optogenetic tools in living organisms.

bioRxiv preprint doi: https://doi.org/10.1101/2021.05.19.444883; this version posted May 28, 2021. The copyright holder for this preprint (which was not certified by peer review) is the author/funder, who has granted bioRxiv a license to display the preprint in perpetuity. It is made available under aCC-BY-NC-ND 4.0 International license.

MATERIALS AND METHODS

Plasmids

The cDNAs of *PcyA*, *HO1*, *Fd*, and *Fnr* were originally derived from *Thermosynechococcus elongatus* BP-1 as previously described (Uda et al., 2020). The mitochondrial targeting sequence (MTS; MSVLTPLLLRGLTGSARRLP) was derived from human cytochrome C oxidase subunit VIII. The cDNAs were subcloned into vectors through conventional ligation with Ligation high Ver.2 (Toyobo, Osaka, Japan) or NEBuilder HiFi DNA Assembly (New England Biolabs, Ipswich, MA) according to the manufacturers' instruction. The nucleotide sequence of mNeonGreen and Turquoise2-GL were optimized for fission yeast codon usage (see Benchling link; Table S1). The pSKI vectors include *Amp*, *colEI ori* (derived from pUC119), selection marker cassettes (derived from pFA6a-3FLAG-bsd, pFA6a-kan, pAV0587 (pHis5Stul-bleMX), pMNATZA1, and pHBCN1), *Padh1*, *Tadh1* (derived from pNATZA1), *Pnmt1*, *Tnmt1* (derived from pREP1), and MCSs (synthesized as oligo DNA (Fasmac)). To construct pSKI-SynPCB2.1-Lifeact-iRFP, *Pact1* (822 bp upstream of the start codon) was cloned from the fission yeast genome, and the cDNA of Lifeact was introduced by ligating annealed oligo DNAs. All plasmids used in this study are listed in Table S1 with Benchling links, which include the sequences and plasmid maps.

Reagents

Biliverdin hydrochloride was purchased from Sigma-Aldrich (30891-50MG), dissolved in DMSO (25 mM stock solution and a final concentration ranging from 8 nM to 625 μM), and stored at −30°C. PCB was purchased from Santa Cruz Biotechnology (sc-396921), dissolved in DMSO (final concentration, 5 mM), and stored at −30°C.

Fission yeast *Schizosaccharomyces pombe* strain and culture

All strains made and used in this study are listed in Table S2. The growth medium, sporulation medium, and other techniques for fission yeast were based on the protocol described previously (Moreno et al., 1991) unless otherwise noted. The transformation protocol was modified from that of Suga and Hatakeyama, 2005. Genome integration by pSKI was confirmed by colony PCR with KOD One (TOYOBO) and the primers listed in Table S3. For the fluorescence microscope imaging, the fission yeast cells were concentrated by centrifugation at 3,000 rpm, mounted on a slide glass, and sealed by a cover glass (Matsunami).

bioRxiv preprint doi: https://doi.org/10.1101/2021.05.19.444883; this version posted May 28, 2021. The copyright holder for this preprint (which was not certified by peer review) is the author/funder, who has granted bioRxiv a license to display the preprint in perpetuity. It is made available under aCC-BY-NC-ND 4.0 International license.

466

467 **HeLa cell culture**

468 HeLa cells were the kind gift of Michiyuki Matsuda (Kyoto University) and cultured in Dulbecco's
469 Modified Eagle's Medium (DMEM) high glucose (Wako; Nacalai Tesque) supplemented with 10%
470 fetal bovine serum (FBS) (Sigma-Aldrich) at 37°C in 5% CO_2. For the live-cell imaging, HeLa cells
471 were plated on CELLview cell culture dishes (glass bottom, 35 mm diameter, 4 components: The
472 Greiner Bio-One). One day after seeding, transfection was performed with 293fectin transfection
473 reagent (Thermo Fisher Scientific). Two days after transfection, cells were imaged with fluorescence
474 microscopes. BV or PCB was added into the DMEM medium containing 10% FBS and cultured for 3 h
475 at 37°C in 5% CO_2.

476

477 **Measurement of the growth rate of fission yeast**

478 Fission yeast cells were pre-cultured at 30 ℃ up to the optical density at 600 nm (OD600) of 1.0,
479 followed by dilution to 1:100. A Compact Rocking Incubator Biophotorecorder TVS062CA (Advantec,
480 Japan) was used for culture growth (30 ℃, 70 rpm) and OD660 measurement. Growth curves were
481 fitted by the logistic function ($x= K / (1 + (K/x_0 -1)e^{-rt})$), and doubling time ($ln2/ r$) was calculated on
482 Python 3 and Scipy.

483

484 **Protein purification**

485 For the purification of His-tag fused iRFP, pCold-TEV-linker-iRFP was transformed into BL21(DE3)
486 pLysS. *E. coli* (Promega, L1195) and selected on LB plates containing 0.1 mg/ml ampicillin at 37℃
487 overnight. A single colony was picked up and inoculated into 2.5 mL liquid LB medium supplemented
488 with 0.1 mg/ml ampicillin and 30 μg/ml chloramphenicol at 37℃ overnight. The preculture was further
489 inoculated into 250 mL liquid LB medium (1:100) containing ampicillin and chloramphenicol. The
490 culture was shaken at 37℃ for 2–4 h until the OD600 reached 0.6–1.0. The culture was then cooled to
491 18℃ and 0.25 mM Isopropyl β-D-1-thiogalactopyranoside (IPTG) (Wako, 094-05144) was added to
492 induce the expression of His fused protein. After overnight incubation at 18℃, cells were collected and
493 suspended into phosphate–buffered saline (PBS) (Takara, T900) containing 20 mM imidazole (Nacalai
494 Tesque, 19004-22). Suspended cells were lysed sonication (VP-300N; TAITEC), followed by
495 centrifugation to collect the supernatant. The supernatant was mixed with 250 μL Ni-NTA sepharose
496 (Qiagen, 1018244), and incubated at 4℃ for 2 h. Protein-bound beads were washed with PBS
497 containing 20 mM imidazole, and proteins were eluted by the addition of 300 mM imidazole in PBS.

bioRxiv preprint doi: https://doi.org/10.1101/2021.05.19.444883; this version posted May 28, 2021. The copyright holder for this preprint (which was not certified by peer review) is the author/funder, who has granted bioRxiv a license to display the preprint in perpetuity. It is made available under aCC-BY-NC-ND 4.0 International license.

Eluted fractions were checked by SDS-PAGE with a protein molecular weight marker, Precision Plus Protein™ All Blue Standards (Bio-Rad, #1610373), followed by CBB staining (BIOCRAFT, CBB-250) and detection by an Odyssey CLx system (Licor). Protein-containing fractions were dialyzed using a Slide-A-Lyzer Dialysis Cassette 3,500 MWCO (Thermo Scientific, 66110) to remove the imidazole. To concentrate the recombinant protein, Amicon ultra 3K 500 μL (Millipore, UFC500308) was used. To measure the protein concentration, Pierce™ BCA Protein Assay Kit (Thermo Scientific, 23227) was used. Purified His-iRFP was mixed with an excess amount of BV or PCB (1:5 molar ratio), followed by size exclusion chromatography with NAP-5 Columns (Cytiva, 17085301) to remove free BV or PCB.

Characterization of *in vitro* fluorescence properties

The absorption of BV (100 μM), PCB (100 μM), and His-iRFP (12 μM) bound to chromophore was measured by a P330 nanophotometer (IMPLEN) with a 10 mm quartz glass cuvette (TOSOH, T-29M UV10). The absorption spectrum was measured in a wavelength range of 200 nm to 950 nm. For the measurements of absolute fluorescence quantum yield, BV or PCB bound His-iRFP (1 μM) in PBS was subjected to analysis with a Quantaurus-QY C11347-01 system (Hamamatsu Photonics). The excitation wavelength was 640 nm. For the measurements of excitation and emission spectra, BV- or PCB- bound His-iRFP (12 μM) was subjected to analysis with an F-4500 fluorescence spectrophotometer (Hitachi). The protein solution was excited in a wavelength range of 500 nm to 720 nm, and fluorescence at 730 nm was detected to measure the excitation spectrum. To measure the emission spectrum, the protein solution was excited at 640 nm, and fluorescence was detected in a wavelength range of 660 nm to 800 nm.

Measurement of *in vivo* emission spectrum

The lambda-scan function of the Leica SP8 Falcon confocal microscope system was used for measurement of the fluorescence emission spectrum. The excitation wavelength was fixed at 633 nm, and the 20 nm emission window was slid in 3 nm increments from 650 nm to 768 nm. Each emission spectrum was normalized by the peak emission value.

Live-cell fluorescence imaging

Cells were imaged with an IX83 inverted microscope (Olympus) equipped with an sCMOS camera (ORCA-Fusion BT; Hamamatsu Photonics), an oil objective lens (UPLXAPO 100X, NA = 1.45, WD = 0.13 mm or

bioRxiv preprint doi: https://doi.org/10.1101/2021.05.19.444883; this version posted May 28, 2021. The copyright holder for this preprint (which was not certified by peer review) is the author/funder, who has granted bioRxiv a license to display the preprint in perpetuity. It is made available under aCC-BY-NC-ND 4.0 International license.

UPLXAPO 60X, NA = 1.42, WD = 0.15 mm; Olympus), and a spinning disk confocal unit (CSU-W1; Yokogawa Electric Corporation). The excitation laser and fluorescence filter settings were as follows: excitation laser, 488 nm and 640 nm for mNeonGreen (or EGFP) and iRFP, respectively; excitation dichroic mirror, DM405/488/561/640; emission filters, 525/50 for mNeonGreen or EGFP, and 685/40 for iRFP (Yokogawa Electric). For the five color multiplexed imaging, cells were imaged with Leica SP8 Falcon (Leica) equipped with an oil objective lens (HCPL APO CS2 100x/1.40 OIL). The excitation laser and fluorescence detectors settings were as follows: excitation laser, 405 nm, 470 nm, 488 nm, 560 nm, and 633 nm for mTagBFP2, Turquoise2-GL, mNeonGreen, mCherry, and iRFP, respectively; detector bandwidth, 420-450 nm, 480-500 nm, 500-550 nm, 580-650 nm, and 680-780 nm for mTagBFP2, Turquoise2-GL, mNeonGreen, mCherry, and iRFP, respectively. Images were obtained with 10 Z-slices of 0.5 μm intervals. Images were subjected to deconvolution by Lightning (Leica).

Imaging analysis

All fluorescence imaging data were analyzed and quantified by Fiji (Image J). The background was subtracted by the rolling-ball method. Some images were obtained with 10–30 Z-slices of 0.2 μm intervals and shown as 2D images by the maximal intensity projection as noted in each figure legend. For the quantification of signal intensity, appropriate ROIs were manually selected, and mean intensities in ROIs were measured.

Analysis of *HO*-like sequences in representative species

We searched for *HO*-like sequences in representative fungal species using BLASTp (for details see Table S4). We adopted human *HO1* (Uniprot P09601) and *S. cerevisiae HMX1* (Uniprot P32339) as the queries (e-value < 1e-5). The phylogenetic relationship is based on recent studies using multiple genes (Li et al., 2021; Nguyen et al., 2017). Since the results suggested sequence divergence among *HO1* homologues, we also used HO-like proteins of *Laccaria bicolor* and *Saitoella complicata* obtained from the BLASTp hits, although no additional sequence was found. Note that the absence in *Aspergillus nidulans* and the existence in *Candida albicans* are consistent with previous studies (Blumenstein et al., 2005; Pendrak et al., 2004). Concerning *C. elegans*, we searched for *HO-like sequence* by the BLASTp interface provided on the WormBase web site (http://www.wormbase.org, release WS280, date 20-Dec-2020, database version WS279). We used the same protein queries, *i.e.*, human *HO1* and *S. cerevisiae HMX1*, although we obtained no hits (e-value < 1e-2).

bioRxiv preprint doi: https://doi.org/10.1101/2021.05.19.444883; this version posted May 28, 2021. The copyright holder for this preprint (which was not certified by peer review) is the author/funder, who has granted bioRxiv a license to display the preprint in perpetuity. It is made available under aCC-BY-NC-ND 4.0 International license.

Acknowledgments

We thank all members of the Aoki Laboratory for their helpful discussions and assistance. The pCold-TEV plasmid was a kind gift of Dr. Koichi Kato (ExCELLS). Some fission yeast strains were provided by the National Bio-Resource Project (NBRP), Japan. We thank the Functional Genomics Facility of the NIBB Core Research Facilities for their technical support with the fluorescence spectrometry.

Competing Interests

The authors declare no competing or financial interest.

Author contributions

Conceptualization: Y.G.; Data curation: Y.G., K.S., Y.K.; Formal analysis: Y.G., K.S., Y.K.; Funding acquisition: Y.K., M.K., Y.G., K.A.; Investigation: Y.G., K.S., Y.K., H.F, M.K.; Methodology: Y.G., K.S., Y.K., H.F, M.K.; Project administration: Y.G., K.A.; Resources: Y.G., K.S., H.F, M.K.; Supervision: K.A., Y.G.; Visualization: Y.G., K.S., Y.K.; Validation: Y.G., K.S., Y.K.; Writing - original draft: Y.G., K.S., Y.K., K.A.; Writing - review & editing: Y.G., K.S., Y.K., K.A.

Funding

K.A. was supported by a CREST, JST Grant (JPMJCR1654), JSPS KAKENHI Grants (nos. 18H02444 and 19H05798), and the ONO Medical Research Foundation. Y.G. was supported by a JSPS KAKENHI Grant (no.19K16050), a Jigami Yoshifumi Memorial Research Grant, and a Sumitomo Research grant. Y.K. was supported by JSPS KAKENHI Grants (nos. 19K16207 and 19H05675).

bioRxiv preprint doi: https://doi.org/10.1101/2021.05.19.444883; this version posted May 28, 2021. The copyright holder for this preprint (which was not certified by peer review) is the author/funder, who has granted bioRxiv a license to display the preprint in perpetuity. It is made available under aCC-BY-NC-ND 4.0 International license.

References

Blumenstein, A., Vienken, K., Tasler, R., Purschwitz, J., Veith, D., Frankenberg-Dinkel, N. and Fischer, R. (2005). The Aspergillus nidulans phytochrome FphA represses sexual development in red light. *Curr. Biol.* **15**, 1833–1838.

Chernov, K. G., Redchuk, T. A., Omelina, E. S. and Verkhusha, V. V. (2017). Near-Infrared Fluorescent Proteins, Biosensors, and Optogenetic Tools Engineered from Phytochromes. *Chem. Rev.* **117**, 6423–6446.

Ding, W.-L., Miao, D., Hou, Y.-N., Jiang, S.-P., Zhao, B.-Q., Zhou, M., Scheer, H. and Zhao, K.-H. (2017). Small monomeric and highly stable near-infrared fluorescent markers derived from the thermophilic phycobiliprotein, ApcF2. *Biochim. Biophys. Acta Mol. Cell Res.* **1864**, 1877–1886.

Fennessy, D., Grallert, A., Krapp, A., Cokoja, A., Bridge, A. J., Petersen, J., Patel, A., Tallada, V. A., Boke, E., Hodgson, B., et al. (2014). Extending the Schizosaccharomyces pombe molecular genetic toolbox. *PLoS One* **9**, e97683.

Filonov, G. S., Piatkevich, K. D., Ting, L.-M., Zhang, J., Kim, K. and Verkhusha, V. V. (2011). Bright and stable near-infrared fluorescent protein for in vivo imaging. *Nat. Biotechnol.* **29**, 757–761.

Froehlich, A. C., Noh, B., Vierstra, R. D., Loros, J. and Dunlap, J. C. (2005). Genetic and molecular analysis of phytochromes from the filamentous fungus Neurospora crassa. *Eukaryot. Cell* **4**, 2140–2152.

Fushimi, K. and Narikawa, R. (2021). Phytochromes and Cyanobacteriochromes: Photoreceptor Molecules Incorporating a Linear Tetrapyrrole Chromophore. In *Optogenetics: Light-Sensing Proteins and Their Applications in Neuroscience and Beyond* (ed. Yawo, H.), Kandori, H.), Koizumi, A.), and Kageyama, R.), pp. 167–187. Singapore: Springer Singapore.

Fushimi, K., Miyazaki, T., Kuwasaki, Y., Nakajima, T., Yamamoto, T., Suzuki, K., Ueda, Y., Miyake, K., Takeda, Y., Choi, J.-H., et al. (2019). Rational conversion of chromophore selectivity of cyanobacteriochromes to accept mammalian intrinsic biliverdin. *Proc. Natl. Acad. Sci. U. S. A.* **116**, 8301–8309.

Gambetta, G. A. and Lagarias, J. C. (2001). Genetic engineering of phytochrome biosynthesis in bacteria. *Proc. Natl. Acad. Sci. U. S. A.* **98**, 10566–10571.

Geller, S. H., Antwi, E. B., Di Ventura, B. and McClean, M. N. (2019). Optogenetic Repressors of Gene Expression in Yeasts Using Light-Controlled Nuclear Localization. *Cell. Mol. Bioeng.* **12**, 511–528.

Hochrein, L., Machens, F., Messerschmidt, K. and Mueller-Roeber, B. (2017). PhiReX: a programmable and red light-regulated protein expression switch for yeast. *Nucleic Acids Res.* **45**, 9193–9205.

Kaberniuk, A. A., Shemetov, A. A. and Verkhusha, V. V. (2016). A bacterial phytochrome-based optogenetic system controllable with near-infrared light. *Nat. Methods* **13**, 591–597.

bioRxiv preprint doi: https://doi.org/10.1101/2021.05.19.444883; this version posted May 28, 2021. The copyright holder for this preprint (which was not certified by peer review) is the author/funder, who has granted bioRxiv a license to display the preprint in perpetuity. It is made available under aCC-BY-NC-ND 4.0 International license.

Kakui, Y., Sunaga, T., Arai, K., Dodgson, J., Ji, L., Csikász-Nagy, A., Carazo-Salas, R. and Sato, M. (2015). Module-based construction of plasmids for chromosomal integration of the fission yeast Schizosaccharomyces pombe. *Open Biol.* **5**, 150054.

Kamper, M., Ta, H., Jensen, N. A., Hell, S. W. and Jakobs, S. (2018). Near-infrared STED nanoscopy with an engineered bacterial phytochrome. *Nat. Commun.* **9**, 4762.

Keeney, J. B. and Boeke, J. D. (1994). Efficient targeted integration at leu1-32 and ura4-294 in Schizosaccharomyces pombe. *Genetics* **136**, 849–856.

Kobachi, K., Kuno, S., Sato, S., Sumiyama, K., Matsuda, M. and Terai, K. (2020). Biliverdin Reductase-A Deficiency Brighten and Sensitize Biliverdin-binding Chromoproteins. *Cell Struct. Funct.* **45**, 131–141.

Kyriakakis, P., Catanho, M., Hoffner, N., Thavarajah, W., Hu, V. J., Chao, S.-S., Hsu, A., Pham, V., Naghavian, L., Dozier, L. E., et al. (2018). Biosynthesis of Orthogonal Molecules Using Ferredoxin and Ferredoxin-NADP+ Reductase Systems Enables Genetically Encoded PhyB Optogenetics. *ACS Synth. Biol.* **7**, 706–717.

Lambert, T. J. (2019). FPbase: a community-editable fluorescent protein database. *Nat. Methods* **16**, 277–278.

Landgraf, F. T., Forreiter, C., Hurtado Picó, A., Lamparter, T. and Hughes, J. (2001). Recombinant holophytochrome in Escherichia coli. *FEBS Lett.* **508**, 459–462.

Lehtivuori, H., Rissanen, I., Takala, H., Bamford, J., Tkachenko, N. V. and Ihalainen, J. A. (2013). Fluorescence properties of the chromophore-binding domain of bacteriophytochrome from Deinococcus radiodurans. *J. Phys. Chem. B* **117**, 11049–11057.

Li, Y., Jin, M., O'Laughlin, R., Bittihn, P., Tsimring, L. S., Pillus, L., Hasty, J. and Hao, N. (2017). Multigenerational silencing dynamics control cell aging. *Proc. Natl. Acad. Sci. U. S. A.* **114**, 11253–11258.

Li, Y., Steenwyk, J. L., Chang, Y., Wang, Y., James, T. Y., Stajich, J. E., Spatafora, J. W., Groenewald, M., Dunn, C. W., Hittinger, C. T., et al. (2021). A genome-scale phylogeny of the kingdom Fungi. *Curr. Biol.* **31**, 1653–1665.e5.

Longtine, M. S., McKenzie, A., 3rd, Demarini, D. J., Shah, N. G., Wach, A., Brachat, A., Philippsen, P. and Pringle, J. R. (1998). Additional modules for versatile and economical PCR-based gene deletion and modification in Saccharomyces cerevisiae. *Yeast* **14**, 953–961.

Loughlin, P. C., Duxbury, Z., Mugerwa, T. T. M., Smith, P. M. C., Willows, R. D. and Chen, M. (2016). Spectral properties of bacteriophytochrome AM1_5894 in the chlorophyll d-containing cyanobacterium Acaryochloris marina. *Sci. Rep.* **6**, 27547.

Matlashov, M. E., Shcherbakova, D. M., Alvelid, J., Baloban, M., Pennacchietti, F., Shemetov, A. A., Testa, I. and Verkhusha, V. V. (2020). A set of monomeric near-infrared fluorescent proteins for multicolor imaging across scales. *Nat. Commun.* **11**, 239.

bioRxiv preprint doi: https://doi.org/10.1101/2021.05.19.444883; this version posted May 28, 2021. The copyright holder for this preprint (which was not certified by peer review) is the author/funder, who has granted bioRxiv a license to display the preprint in perpetuity. It is made available under aCC-BY-NC-ND 4.0 International license.

Matsuyama, A., Shirai, A., Yashiroda, Y., Kamata, A., Horinouchi, S. and Yoshida, M. (2004). pDUAL, a multipurpose, multicopy vector capable of chromosomal integration in fission yeast. *Yeast* **21**, 1289–1305.

Maundrell, K. (1993). Thiamine-repressible expression vectors pREP and pRIP for fission yeast. *Gene* **123**, 127–130.

Monakhov, M. V., Matlashov, M. E., Colavita, M., Song, C., Shcherbakova, D. M., Antic, S. D., Verkhusha, V. V. and Knöpfel, T. (2020). Screening and Cellular Characterization of Genetically Encoded Voltage Indicators Based on Near-Infrared Fluorescent Proteins. *ACS Chem. Neurosci.* **11**, 3523–3531.

Moreno, S., Klar, A. and Nurse, P. (1991). Molecular genetic analysis of fission yeast Schizosaccharomyces pombe. *Methods Enzymol.* **194**, 795–823.

Mukougawa, K., Kanamoto, H., Kobayashi, T., Yokota, A. and Kohchi, T. (2006). Metabolic engineering to produce phytochromes with phytochromobilin, phycocyanobilin, or phycoerythrobilin chromophore in Escherichia coli. *FEBS Lett.* **580**, 1333–1338.

Müller, K., Engesser, R., Timmer, J., Nagy, F., Zurbriggen, M. D. and Weber, W. (2013). Synthesis of phycocyanobilin in mammalian cells. *Chem. Commun.* **49**, 8970–8972.

Nguyen, T. A., Cissé, O. H., Yun Wong, J., Zheng, P., Hewitt, D., Nowrousian, M., Stajich, J. E. and Jedd, G. (2017). Innovation and constraint leading to complex multicellularity in the Ascomycota. *Nat. Commun.* **8**, 14444.

Oliinyk, O. S., Shemetov, A. A., Pletnev, S., Shcherbakova, D. M. and Verkhusha, V. V. (2019). Smallest near-infrared fluorescent protein evolved from cyanobacteriochrome as versatile tag for spectral multiplexing. *Nat. Commun.* **10**, 279.

Pendrak, M. L., Chao, M. P., Yan, S. S. and Roberts, D. D. (2004). Heme Oxygenase in Candida albicans Is Regulated by Hemoglobin and Is Necessary for Metabolism of Exogenous Heme and Hemoglobin to α-Biliverdin*. *J. Biol. Chem.* **279**, 3426–3433.

Piatkevich, K. D., Suk, H.-J., Kodandaramaiah, S. B., Yoshida, F., DeGennaro, E. M., Drobizhev, M., Hughes, T. E., Desimone, R., Boyden, E. S. and Verkhusha, V. V. (2017). Near-Infrared Fluorescent Proteins Engineered from Bacterial Phytochromes in Neuroimaging. *Biophys. J.* **113**, 2299–2309.

Qian, Y., Cosio, D. M. O., Piatkevich, K. D., Aufmkolk, S., Su, W.-C., Celiker, O. T., Schohl, A., Murdock, M. H., Aggarwal, A., Chang, Y.-F., et al. (2020). Improved genetically encoded near-infrared fluorescent calcium ion indicators for in vivo imaging. *PLoS Biol.* **18**, e3000965.

Redchuk, T. A., Omelina, E. S., Chernov, K. G. and Verkhusha, V. V. (2017). Near-infrared optogenetic pair for protein regulation and spectral multiplexing. *Nat. Chem. Biol.* **13**, 633–639.

Regot, S., Hughey, J. J., Bajar, B. T., Carrasco, S. and Covert, M. W. (2014). High-sensitivity measurements of multiple kinase activities in live single cells. *Cell* **157**, 1724–1734.

bioRxiv preprint doi: https://doi.org/10.1101/2021.05.19.444883; this version posted May 28, 2021. The copyright holder for this preprint (which was not certified by peer review) is the author/funder, who has granted bioRxiv a license to display the preprint in perpetuity. It is made available under aCC-BY-NC-ND 4.0 International license.

Rhie, G. and Beale, S. I. (1992). Biosynthesis of phycobilins. Ferredoxin-supported nadph-independent heme oxygenase and phycobilin-forming activities from Cyanidium caldarium. *J. Biol. Chem.* **267**, 16088–16093.

Rodriguez, E. A., Tran, G. N., Gross, L. A., Crisp, J. L., Shu, X., Lin, J. Y. and Tsien, R. Y. (2016). A far-red fluorescent protein evolved from a cyanobacterial phycobiliprotein. *Nat. Methods* **13**, 763–769.

Rogers, O. C., Johnson, D. M. and Firnberg, E. (2019). mRhubarb: Engineering of monomeric, red-shifted, and brighter variants of iRFP using structure-guided multi-site mutagenesis. *Sci. Rep.* **9**, 15653.

Rumyantsev, K. A., Shcherbakova, D. M., Zakharova, N. I., Emelyanov, A. V., Turoverov, K. K. and Verkhusha, V. V. (2015). Minimal domain of bacterial phytochrome required for chromophore binding and fluorescence. *Sci. Rep.* **5**, 18348.

Shcherbakova, D. M. and Verkhusha, V. V. (2013). Near-infrared fluorescent proteins for multicolor in vivo imaging. *Nat. Methods* **10**, 751–754.

Shcherbakova, D. M., Baloban, M., Emelyanov, A. V., Brenowitz, M., Guo, P. and Verkhusha, V. V. (2016). Bright monomeric near-infrared fluorescent proteins as tags and biosensors for multiscale imaging. *Nat. Commun.* **7**, 12405.

Shcherbakova, D. M., Cox Cammer, N., Huisman, T. M., Verkhusha, V. V. and Hodgson, L. (2018). Direct multiplex imaging and optogenetics of Rho GTPases enabled by near-infrared FRET. *Nat. Chem. Biol.* **14**, 591–600.

Shemetov, A. A., Oliinyk, O. S. and Verkhusha, V. V. (2017). How to Increase Brightness of Near-Infrared Fluorescent Proteins in Mammalian Cells. *Cell Chem Biol* **24**, 758–766.e3.

Shin, A.-Y., Han, Y.-J., Song, P.-S. and Kim, J.-I. (2014). Expression of recombinant full-length plant phytochromes assembled with phytochromobilin in Pichia pastoris. *FEBS Lett.* **588**, 2964–2970.

Siam, R., Dolan, W. P. and Forsburg, S. L. (2004). Choosing and using Schizosaccharomyces pombe plasmids. *Methods* **33**, 189–198.

Stepanenko, O. V., Baloban, M., Bublikov, G. S., Shcherbakova, D. M., Stepanenko, O. V., Turoverov, K. K., Kuznetsova, I. M. and Verkhusha, V. V. (2016). Allosteric effects of chromophore interaction with dimeric near-infrared fluorescent proteins engineered from bacterial phytochromes. *Sci. Rep.* **6**, 18750.

Suga, M. and Hatakeyama, T. (2005). A rapid and simple procedure for high-efficiency lithium acetate transformation of cryopreserved Schizosaccharomyces pombe cells. 799–804.

Terry, M. J., Maines, M. D. and Lagarias, J. C. (1993). Inactivation of phytochrome- and phycobiliprotein-chromophore precursors by rat liver biliverdin reductase. *J. Biol. Chem.* **268**, 26099–26106.

bioRxiv preprint doi: https://doi.org/10.1101/2021.05.19.444883; this version posted May 28, 2021. The copyright holder for this preprint (which was not certified by peer review) is the author/funder, who has granted bioRxiv a license to display the preprint in perpetuity. It is made available under aCC-BY-NC-ND 4.0 International license.

Tojima, T., Suda, Y., Ishii, M., Kurokawa, K. and Nakano, A. (2019). Spatiotemporal dissection of the trans-Golgi network in budding yeast. *J. Cell Sci.* **132**,.

Tooley, A. J., Cai, Y. A. and Glazer, A. N. (2001). Biosynthesis of a fluorescent cyanobacterial C-phycocyanin holo-α subunit in a heterologous host. *Proc. Natl. Acad. Sci. U. S. A.* **98**, 10560–10565.

Uda, Y., Goto, Y., Oda, S., Kohchi, T., Matsuda, M. and Aoki, K. (2017). Efficient synthesis of phycocyanobilin in mammalian cells for optogenetic control of cell signaling. *Proc. Natl. Acad. Sci. U. S. A.* **114**, 11962–11967.

Uda, Y., Miura, H., Goto, Y., Yamamoto, K., Mii, Y., Kondo, Y., Takada, S. and Aoki, K. (2020). Improvement of Phycocyanobilin Synthesis for Genetically Encoded Phytochrome-Based Optogenetics. *ACS Chem. Biol.*

Vještica, A., Marek, M., Nkosi, P. J., Merlini, L., Liu, G., Bérard, M., Billault-Chaumartin, I. and Martin, S. G. (2020). A toolbox of stable integration vectors in the fission yeast Schizosaccharomyces pombe. *J. Cell Sci.* **133**,.

Wagner, J. R., Zhang, J., von Stetten, D., Günther, M., Murgida, D. H., Mroginski, M. A., Walker, J. M., Forest, K. T., Hildebrandt, P. and Vierstra, R. D. (2008). Mutational analysis of Deinococcus radiodurans bacteriophytochrome reveals key amino acids necessary for the photochromicity and proton exchange cycle of phytochromes. *J. Biol. Chem.* **283**, 12212–12226.

Wosika, V., Durandau, E., Varidel, C., Aymoz, D., Schmitt, M. and Pelet, S. (2016). New families of single integration vectors and gene tagging plasmids for genetic manipulations in budding yeast. *Mol. Genet. Genomics* **291**, 2231–2240.

Yu, D., Gustafson, W. C., Han, C., Lafaye, C., Noirclerc-Savoye, M., Ge, W.-P., Thayer, D. A., Huang, H., Kornberg, T. B., Royant, A., et al. (2014). An improved monomeric infrared fluorescent protein for neuronal and tumour brain imaging. *Nat. Commun.* **5**, 3626.

Yu, D., Baird, M. A., Allen, J. R., Howe, E. S., Klassen, M. P., Reade, A., Makhijani, K., Song, Y., Liu, S., Murthy, Z., et al. (2015). A naturally monomeric infrared fluorescent protein for protein labeling in vivo. *Nat. Methods* **12**, 763–765.